

# Evaluation of the beam-induced depolarization of the HJET target at the EIC

A. A. Poblagev\*

Brookhaven National Laboratory, Upton, New York 11973, USA

## Abstract

The Polarized Atomic Hydrogen Gas Jet Target (HJET) has played a central role in the absolute calibration of proton beam polarization at RHIC and is foreseen as a key element of the hadron polarimetry program at the future Electron–Ion Collider (EIC). The substantially higher beam current, reduced bunch spacing, and shorter bunch length planned for EIC operation motivate a careful reassessment of possible beam-induced depolarization of the jet target. In this paper, the depolarization of ground-state hydrogen atoms caused by the time-dependent magnetic field of the circulating polarized proton beam is quantitatively evaluated. The hydrogen atom is treated as a four-level hyperfine system in a holding magnetic field, and transitions driven by harmonic components of the bunch-induced magnetic field are analyzed using time-dependent quantum-mechanical evolution along atomic trajectories. Numerical tracking of hydrogen atoms through the beam region is performed using nominal EIC beam parameters. It is shown that, for a holding field of 120 mT (as used at RHIC), the resulting depolarization of the jet target at the EIC is negligibly small,  $\lesssim 0.01\%$ , and well below the level relevant for EIC polarization accuracy requirements. The stability of this result with respect to plausible variations of the EIC proton beam parameters is also evaluated.

**Keywords:** Electron–Ion Collider, Hadron polarimetry, Polarized hydrogen target, Beam-induced depolarization, Breit–Rabi polarimeter

## 1. Introduction

High-energy 41–275 GeV polarized ( $\gtrsim 70\%$ ) proton beams are planned for the Electron–Ion Collider (EIC) [1, 2]. The Science Requirements for hadron polarimetry at the EIC [3] include a precise calibration of the measured proton beam polarization, with systematic uncertainties better than

$$\sigma_P^{\text{syst}}/P \lesssim 1\%. \quad (1)$$

Since hadron polarimetry at the Relativistic Heavy-Ion Collider (RHIC) has been successfully performed for more than two decades, it is considered a natural starting point for the EIC hadron polarimetry program.

Within the RHIC Spin Program [4, 5], several polarimeters are employed, including the 200 MeV absolute proton–carbon polarimeter at the LINAC [6, 7], the relative proton–carbon recoil polarimeters [8] at the AGS and RHIC, and the Polarized Atomic Hydrogen Gas Jet Target (HJET) [9, 10]. These instruments are used to monitor the beam polarization and to provide essential information to the RHIC experiments, such as the polarization value, polarization profile, proton spin tilt, and polarization decay time. The primary role of the HJET is the precise absolute calibration of the proton beam polarization.

During polarized proton runs at RHIC, the systematic uncertainty of the measured proton beam polarization was evaluated to be  $\sigma_P^{\text{syst}}/P \sim 0.5\%$  [11, 10], which satisfies the EIC requirement given by Eq. (1).

As shown in Table 1, at the EIC the beam current will be increased by more than a factor of three compared to RHIC, while the bunch spacing and the bunch length will be reduced by nearly an order of magnitude. Consequently, a reassessment of the HJET performance under the new operating conditions is required.

Possible effects of the short bunch spacing on proton beam polarization measurements with the HJET recoil spectrometer were previously evaluated in Refs. [13, 14] using an emulation of the EIC bunch structure based on HJET experimental data obtained at RHIC. In these studies, however, the jet target polarization—which is determined, under certain assumptions, by the HJET Breit–Rabi polarimeter (BRP)—was assumed to be well known.

In the present paper, we focus on an evaluation of beam-induced depolarization [15] of the jet target itself. In such a study, it is essential to compare the depolarization effects relevant for the recoil spectrometer with those affecting the BRP. Therefore, the paper also includes a discussion of basic HJET design-related systematic effects relevant to these measurements.

As a prerequisite, a brief description of the hyperfine structure of a ground-state hydrogen atom in the holding-field magnet is given in Section 2. The RHIC HJET design and performance, including a discussion of the optimization of the BRP measurement algorithm, are reviewed in Section 3. The methodology used to evaluate beam-induced depolarization is described in Section 4. In Section 5, it is shown that the expected depolarization of the HJET target at the EIC is negli-

\*Corresponding author

Email address: [poblagev@bnl.gov](mailto:poblagev@bnl.gov) (A. A. Poblagev)

Table 1: Beam parameters essential for the evaluation of beam-induced depolarization for RHIC flattop and for EIC injection and flattop nominal conditions [12]. For both machines, the circumference is 3833.85 m. IP 12 and IP 4 denote the interaction points where the HJET is located at RHIC and will be located at the EIC, respectively. For simplicity, the transverse beam profile at the EIC is approximated in this paper by a round distribution with rms radius  $\sigma_r = (\sigma_x \sigma_y)^{1/2}$ .

Parameter	Notation	Unit	RHIC at IP 12	EIC at IP 4	
			flattop	injection	flattop
Beam energy	$E_{\text{beam}}$	GeV	255	23.5	275
Number of bunches	$N_b$	–	120	290	1160
Protons per bunch	$N_p$	$10^{10}$	20	27.6	6.9
Temporal bunch length	$\sigma_t$	ns	1.835	0.801	0.200
Bunch spacing	$\tau_b$	ns	106.598	44.144	11.027
Bunch frequency	$f_b$	MHz	9.381	22.653	90.683
Average beam current	$I_{\text{avg}}$	A	0.301	1.002	1.003
Transverse beam size	$\sigma_x$	mm	–	3.513	1.610
	$\sigma_y$	mm	–	0.689	0.268
Radial beam size	$\sigma_r$	mm	0.23	1.566	0.656

gibly small. Finally, the stability of this result with respect to plausible variations of the proton beam parameters is discussed in Section 6.

## 2. The hyperfine structure of the ground-state hydrogen

The hyperfine structure of the hydrogen atom ground state in an external magnetic field  $\mathbf{B}$  is described by the electron– and proton–spin–dependent Hamiltonian, which can be written in terms of Pauli matrices as [16]

$$H_0 = E_0 + \frac{E_{\text{hfs}}}{4} \boldsymbol{\sigma}^e \cdot \boldsymbol{\sigma}^p - (\mu_e \boldsymbol{\sigma}^e + \mu_p \boldsymbol{\sigma}^p) \cdot \mathbf{B}, \quad (2)$$

where  $\mu_e$  and  $\mu_p$  are the magnetic moments of the electron and proton, respectively. Numerically [17],

$$\frac{\mu_e}{2\pi\hbar} = -14.012 \text{ MHz/mT}, \quad \frac{\mu_p}{2\pi\hbar} = 0.021 \text{ MHz/mT}. \quad (3)$$

In the following, the proton magnetic moment is neglected.

Due to the electromagnetic multipole interaction between the proton and the electron cloud, the ground state of the hydrogen atom is split into sublevels characterized by the total atomic angular momentum quantum number  $F$ : a triplet state ( $F = 1$ ) and a singlet state ( $F = 0$ ), as illustrated in Fig. 1. The separation between the  $F = 1$  and  $F = 0$  levels is known with very high precision [18],

$$\frac{E_{\text{hfs}}}{2\pi\hbar} = f_{\text{hfs}} = 14230405748.4 \pm 3.4_{\text{stat}} \pm 1.6_{\text{syst}} \text{ Hz}, \quad (4)$$

where  $\hbar$  is the reduced Planck constant. In energy units, this corresponds to  $E_{\text{hfs}} \approx 5.9 \times 10^{-6} \text{ eV}$ .

In the presence of a holding magnetic field  $B_{\text{hold}}$ , the triplet state undergoes Zeeman splitting. The corresponding energy

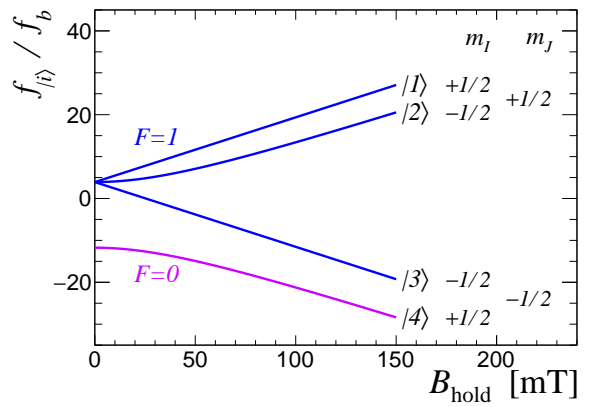


Figure 1: Breit-Rabi diagram for ground-state hydrogen ( $1S_{1/2}$ ). The projection of the total spin  $F$  onto the holding magnetic field  $B_{\text{hold}}$  is given by  $m_F = m_l + m_J$ , where  $m_l$  and  $m_J$  are the proton and electron spin projections, respectively, in the high-field limit ( $\sin \theta \rightarrow 0$  in Eq. (7)).

levels, expressed in frequency units, can be approximated as

$$\begin{aligned} f_{|1\rangle}(B_{\text{hold}}) &= \frac{f_{\text{hfs}}}{2} \left( -\frac{1}{2} + (1 + x) \right), \\ f_{|2\rangle}(B_{\text{hold}}) &= \frac{f_{\text{hfs}}}{2} \left( -\frac{1}{2} + \sqrt{1 + x^2} \right), \\ f_{|3\rangle}(B_{\text{hold}}) &= \frac{f_{\text{hfs}}}{2} \left( -\frac{1}{2} + (1 - x) \right), \\ f_{|4\rangle}(B_{\text{hold}}) &= \frac{f_{\text{hfs}}}{2} \left( -\frac{1}{2} - \sqrt{1 + x^2} \right), \end{aligned} \quad (5)$$

with

$$x = \frac{B_{\text{hold}}}{B_c}, \quad B_c = \frac{f_{\text{hfs}}}{2|\mu_e/2\pi\hbar|} = 50.7 \text{ mT}. \quad (6)$$

The spin structure of the hyperfine eigenstates and the corre-

sponding nuclear polarizations are given by

$$\begin{aligned} |1\rangle &= |e^\uparrow p^\uparrow\rangle, & P_{|1\rangle} &= +1, \\ |2\rangle &= \cos\theta |e^\uparrow p^\downarrow\rangle + \sin\theta |e^\downarrow p^\uparrow\rangle, & P_{|2\rangle} &= -\cos(2\theta), \\ |3\rangle &= |e^\downarrow p^\downarrow\rangle, & P_{|3\rangle} &= -1, \\ |4\rangle &= \cos\theta |e^\downarrow p^\uparrow\rangle - \sin\theta |e^\uparrow p^\downarrow\rangle, & P_{|4\rangle} &= +\cos(2\theta), \end{aligned} \quad (7)$$

where  $2\theta = \arctan(1/x)$  and  $\uparrow, \downarrow$  denote spin projections along the magnetic-field direction.

A weak external oscillating magnetic field  $\mathbf{B}_{\text{osc}} \cos(\omega t)$  can induce resonant transitions between states  $|i\rangle$  and  $|j\rangle$  if

$$\frac{\omega}{2\pi} = f_{ij}(B_{\text{hold}}) = f_{|i\rangle}(B_{\text{hold}}) - f_{|j\rangle}(B_{\text{hold}}), \quad (8)$$

a mechanism widely used for polarizing atomic hydrogen beams [19]. Conversely, when such a polarized atomic hydrogen beam is employed as a target in the HJET polarimeter, it may be depolarized by the time-dependent magnetic field generated by the circulating proton beam bunches.

### 2.1. External perturbation of a ground-state hydrogen atom

A ground-state hydrogen atom can be treated as a four-level quantum system with eigenstates  $|n\rangle$  and eigenvalues  $E_{|n\rangle}$  of the time-independent Hamiltonian  $H_0$  in Eq. (2). In the presence of a weak time-dependent perturbation  $H_1(t)$ , the Schrödinger equation in the interaction picture leads to coupled equations for the expansion coefficients  $a_n(t)$  [20]:

$$\left[ H_0 + H_1(t) - i\hbar \frac{d}{dt} \right] \sum_n a_n(t) |n\rangle e^{-iE_n t/\hbar} = 0. \quad (9)$$

The time evolution of the atomic state is governed by

$$i\hbar \frac{da_k(t)}{dt} = \sum_n \mathcal{M}_{kn}(t) a_n(t) e^{i\omega_{kn} t}, \quad (10)$$

where  $\mathcal{M}_{kn}(t) = \langle k|H_1(t)|n\rangle$  is the matrix element of the perturbation and  $\omega_{kn} = (E_k - E_n)/\hbar$ . For specified matrix elements and initial conditions  $a_n(0)$ , the system (10) can be solved exactly, for example by numerical integration.

For practical purposes, individual two-level subsystems of Eq. (10) can be considered independently. If, during the total interaction time  $t_{\text{int}}$ , the transition probability between a given pair of states  $|i\rangle \rightarrow |f\rangle$  remains negligibly small,

$$\left| \frac{1}{\hbar} \int_0^t \mathcal{M}_{fi}(t) e^{i\omega_{fi} t} dt \right| < \eta, \quad (11)$$

for all  $t < t_{\text{int}}$ , where  $\eta$  is the required numerical accuracy for solving Eq. (10), the corresponding transition can be safely neglected (e.g. by setting  $\mathcal{M}_{fi}(t) = 0$ ). As shown below, this criterion allows a substantial simplification of the evaluation of the beam-induced depolarization of the HJET target.

For a two-level system subject to an oscillating perturbation  $\mathcal{M}_{fi}(t) = \hbar\omega_R \cos(\omega t)$ , the transition probability can be obtained analytically [21]. For initial conditions  $a_i(0) = 1$  and

$a_f(0) = 0$ , the probability of finding the system in the final state  $|f\rangle$  at time  $t$  is

$$|a_f(t)|^2 = \frac{\omega_R^2}{\omega_R^2 + \Delta\omega^2} \sin^2 \left( \frac{\sqrt{\omega_R^2 + \Delta\omega^2} t}{2} \right), \quad (12)$$

where  $\omega_R$  is the Rabi angular frequency and  $\Delta\omega = \omega - \omega_{fi}$  is the detuning.

In the limit  $\omega_R \ll \omega$  and  $|\Delta\omega| \ll \omega$ , it is convenient to work in a rotating reference frame, defined by  $a_i(t) = \alpha_i(t)e^{-i\omega t}$  and  $a_f(t) = \alpha_f(t)e^{i\omega t}$ . The two-level system then obeys

$$\begin{aligned} i \frac{d\alpha_i(t)}{dt} &= -\frac{\Delta\omega}{2} \alpha_i(t) + \frac{\omega_R}{2} \alpha_f(t), \\ i \frac{d\alpha_f(t)}{dt} &= \frac{\omega_R}{2} \alpha_i(t) + \frac{\Delta\omega}{2} \alpha_f(t). \end{aligned} \quad (13)$$

For  $\alpha_i(0) = 1$  and  $\alpha_f(0) = 0$ , and *time-independent*  $\omega_R$  and  $\Delta\omega$ , the solution can be readily derived:

$$\alpha_i(t) = \cos\left(\frac{\Omega t}{2}\right) + i \frac{\Delta\omega}{\Omega} \sin\left(\frac{\Omega t}{2}\right), \quad (14)$$

$$\alpha_f(t) = i \frac{\omega_R}{\Omega} \sin\left(\frac{\Omega t}{2}\right), \quad (15)$$

where the generalized Rabi frequency is defined as

$$\Omega = \sqrt{\omega_R^2 + \Delta\omega^2}. \quad (16)$$

This result is fully consistent with Eq. (12).

For a hydrogen atom traversing the proton beam in the HJET, both  $\omega_R(t)$  and  $\Delta\omega(t)$  are, in general, time-dependent. Consequently, Eq. (12) can be used only for preliminary estimates, while the full time-dependent problem must be addressed by numerical integration.

## 3. The RHIC HJET

The RHIC HJET polarimeter [9, 22] consists of nine vertically arranged pumping stages (chambers), as depicted in Fig. 2. The three main components of the polarimeter are the Atomic Beam Source (ABS, chambers 1–5), the recoil spectrometer (chamber 6), and the Breit–Rabi polarimeter (BRP, chambers 7–9). A powerful vacuum system, combined with a carefully designed system of separating magnets, enables delivery of an atomic beam with an intensity of  $1.2 \times 10^{17}$  atoms/s. The atomic beam is focused at the collision point, where the jet thickness is approximately  $1.2 \times 10^{12}$  atoms/cm<sup>2</sup>, and the transverse profile can be approximated by a Gaussian distribution with  $\sigma \approx 2.6$  mm.

### 3.1. The atomic beam source

The H<sub>2</sub> gas injected into the ABS is dissociated into four nearly equally populated hyperfine states of hydrogen atoms,

$$\text{Dissociator: } \{n_1, n_2, n_3, n_4\}. \quad (17)$$

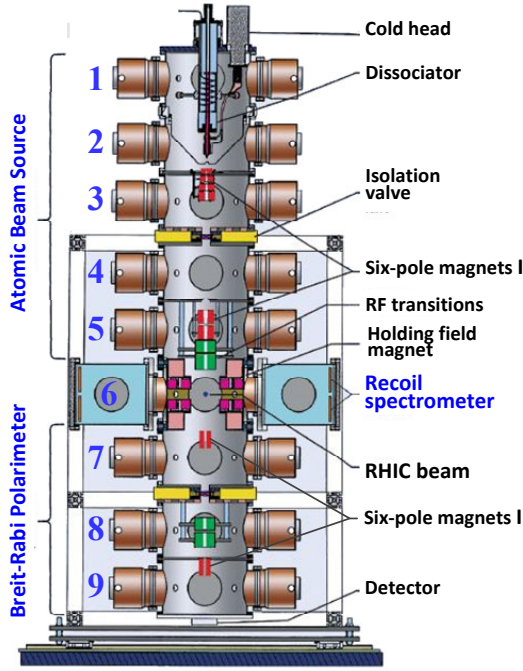


Figure 2: Beam view of the Polarized Atomic Hydrogen Gas Jet target polarimeter at RHIC.

The atoms expand through a cold nozzle and enter the sextupole separating magnet system. Based on the Stern–Gerlach method, the sextupole magnets (with a typical field strength of 1.6–1.7 T) separate atoms with electron spin  $+1/2$  (hyperfine states  $|1\rangle$  and  $|2\rangle$ ) from those with spin  $-1/2$  ( $|3\rangle$  and  $|4\rangle$ ). In addition, the sextupole system focuses the electron spin  $+1/2$  atoms into the target region.

Omitting an overall normalization factor, the atomic-beam hyperfine-state populations at the entrance to the RF transition unit can be approximated as

$$\text{Sep. Magnet I: } \left\{ 1 - \nu, 1 + \nu, \epsilon_l, \epsilon_l \right\}. \quad (18)$$

Here, the parameter  $\nu$  accounts for a small difference in the transmission efficiencies of states  $|1\rangle$  and  $|2\rangle$  through the separating magnet system. In the HJET BRP software, this asymmetry is hard-coded as

$$\frac{n_2}{n_1} = 1.00239 \Rightarrow \nu \approx 0.0012. \quad (19)$$

For comparison, in the HERMES polarized hydrogen target [23], this ratio was experimentally determined to be  $n_2/n_1 = 1.029 \pm 0.0015$ .

The parameter  $\epsilon_l$  in Eq. (18) represents the residual transmission of states  $|3\rangle$  and  $|4\rangle$ ;  $\epsilon_l = 0$  corresponds to an ideal sextupole separating magnet system. For the HJET ABS design, it was estimated [22] that  $\epsilon_l < 0.002$ . Owing to the smallness of  $\epsilon_l$ , no distinction is made between the efficiencies for the  $|3\rangle$  and  $|4\rangle$  states.

If only the Strong Field Transition (SFT), which provides

an adiabatic transition between states  $|2\rangle$  and  $|4\rangle$ , is enabled (SFT=On, WFT=Off), the hyperfine-state populations become

$$\text{SFT: } \left\{ 1 - \nu, (1 + \nu)\epsilon_{24} + \epsilon_l, \epsilon_l, (1 + \nu)(1 - \epsilon_{24}) \right\}, \quad (20)$$

where  $\epsilon_{24}$  denotes the SFT transition inefficiency. Consequently, the atomic hydrogen beam acquires the polarization

$$P_+ = \frac{(1 - \epsilon_l) \cos^2 \theta - \epsilon_{24} \cos 2\theta - \nu (\sin^2 \theta + \epsilon_{24} \cos 2\theta)}{1 + \epsilon_l}. \quad (21)$$

For the RHIC HJET holding field of  $B_{\text{hold}} = 120$  mT,

$$\cos^2 \theta = 0.961, \quad \sin^2 \theta = 0.039, \quad \cos 2\theta = 0.921. \quad (22)$$

Similarly, for the Weak Field Transition configuration (WFT=On, SFT=Off), one obtains

$$\text{WFT: } \left\{ (1 - \nu)\epsilon_{13} + \epsilon_l, 1 + \nu, (1 - \nu)(1 - \epsilon_{13}), \epsilon_l \right\} \quad (23)$$

and

$$-P_- = \frac{(1 - \epsilon_l) \cos^2 \theta - \epsilon_{13} - \nu (\sin^2 \theta - \epsilon_{13})}{1 + \epsilon_l}. \quad (24)$$

At RHIC, the jet target polarization was typically reversed every 300 s during HJET operation. Between periods with hydrogen nuclear spin oriented up and down, both RF transitions (SFT and WFT) were turned on for a short 30 s interval, allowing a BRP-based determination of corrections to the nominal jet polarizations  $\pm \cos^2 \theta$  defined by the holding-field value.

### 3.2. The recoil spectrometer

In the recoil spectrometer, the vertically polarized proton beam, consisting of alternatively polarized bunches, is scattered off the jet target, and the low-energy recoil protons are detected by left/right symmetric silicon detectors located at  $90^\circ$  with respect to the beam direction [10]. The numbers of events counted in the left and right detectors, for different combinations of beam  $(+-)$  and jet  $(\uparrow\downarrow)$  polarizations, allow the determination of the spin-correlated asymmetries for both the beam and the jet:

$$a_{\text{beam}} = \langle A_N^{\text{beam}} \rangle P_{\text{beam}} = \frac{\sqrt{N_R^+ N_L^-} - \sqrt{N_L^+ N_R^-}}{\sqrt{N_R^+ N_L^+} + \sqrt{N_L^+ N_R^-}}, \quad (25)$$

$$a_{\text{jet}} = \langle A_N^{\text{jet}} \rangle P_{\text{jet}} = \frac{\sqrt{N_R^\uparrow N_L^\downarrow} - \sqrt{N_L^\uparrow N_R^\downarrow}}{\sqrt{N_R^\uparrow N_L^\uparrow} + \sqrt{N_L^\uparrow N_R^\downarrow}}. \quad (26)$$

Using analogous expressions with regrouped event numbers  $N_{LR}^{+-}$  and  $N_{LR}^{\uparrow\downarrow}$  [10], one can also determine the beam  $(+-)$  and jet  $(\uparrow\downarrow)$  intensity asymmetries  $\lambda$ , as well as the left–right detector acceptance asymmetry  $\xi$ .

Since identical particles are scattered, the elastic transverse analyzing powers for the beam,  $A_N^{\text{beam}}(t)$ , and for the jet,  $A_N^{\text{jet}}(t)$ , as functions of the momentum transfer  $t$ , are identical. Moreover, if background events are properly eliminated from the  $pp$

elastic-scattering data, one has  $\langle A_N^{\text{beam}} \rangle = \langle A_N^{\text{jet}} \rangle$  [10], because exactly the same events are used to calculate both beam and jet asymmetries. Therefore,

$$P_{\text{beam}} = \frac{a_{\text{beam}}}{a_{\text{jet}}} P_{\text{jet}}. \quad (27)$$

To satisfy the EIC requirement (1), the jet target polarization must be known with an accuracy significantly better than 1%.

Equations (25) and (26) provide a determination of the spin asymmetries  $a$  that is free of systematic errors [10] if (i) the absolute values of the beam (jet) polarizations for spin-up and spin-down states are equal, (ii) the effective analyzing power is the same for the left and right detectors, and (iii) the detector acceptances are independent of the beam (jet) spin direction.

Notably, in the case where

$$\Delta P = |P_+| - |P_-| \neq 0, \quad (28)$$

the calculations based on Eqs. (25) and (26) yield a biased value of the intensity asymmetry,  $\lambda \rightarrow \lambda + \langle A_N \rangle \Delta P$ , while the spin asymmetry itself remains almost unchanged,

$$a \rightarrow a + \frac{a^2}{4} \Delta P. \quad (29)$$

Since in the RHIC and EIC HJET measurements  $a_{\text{beam}} < a_{\text{jet}} \approx 0.04$ , the correction to the measured polarization due to  $\Delta P \neq 0$  is negligibly small even in the extreme case  $|\Delta P| = 1$ . Thus, only spin-direction-averaged values of the beam and jet polarizations are relevant in Eq. (27), and the jet target polarization can be well approximated by

$$P_{\text{jet}} = \frac{|P_+| + |P_-|}{2} = \cos^2 \theta - 2\epsilon_l - \langle \epsilon \rangle, \quad (30)$$

where

$$\langle \epsilon \rangle = \frac{\epsilon_{13} + \epsilon_{24}}{2}. \quad (31)$$

Second-order corrections are omitted in Eq. (30). If

$$|\nu| < 0.05, \quad \epsilon_{13}, \epsilon_{24}, \epsilon_l < 0.01, \quad (32)$$

the corresponding systematic uncertainty in the value of  $P_{\text{jet}}$  is less than 0.1%.

### 3.3. The Breit–Rabi Polarimeter

After passing through the separating and focusing magnet system II, the hydrogen atoms are detected by an ion gauge (the BRP detector).

Depending on the jet polarization state ( $P_+$ ,  $P_-$ , or  $P_0$ ), the signals measured in the ion gauge are proportional to

$$\begin{aligned} m_+ &= (1 - \nu') + (1 + \nu')\epsilon_{24} + \epsilon'_l + \epsilon_{\text{II}} \\ &\approx 1 - \nu' + \epsilon_{24} + \epsilon'_l + \epsilon_{\text{II}} \approx 1, \end{aligned} \quad (33)$$

$$\begin{aligned} m_- &= (1 - \nu')\epsilon_{13} + (1 + \nu') + \epsilon'_l + \epsilon_{\text{II}} \\ &\approx 1 + \nu' + \epsilon_{13} + \epsilon'_l + \epsilon_{\text{II}} \approx 1, \end{aligned} \quad (34)$$

$$\begin{aligned} m_0 &= (1 - \nu')\epsilon_{13} + (1 + \nu')\epsilon_{24} + 2\epsilon'_l + 2\epsilon_{\text{II}} \\ &\approx 2[\langle \epsilon \rangle + \epsilon'_l + \epsilon_{\text{II}}]. \end{aligned} \quad (35)$$

Here,  $\nu'$  and  $\epsilon'_l$  are modified values of  $\nu$  and  $\epsilon_l$  that account for transmission efficiencies in the separating magnet system II, and  $\epsilon_{\text{II}}$  represents the inefficiency of suppressing the electron spin  $-1/2$  states in this system. The second-order terms in Eqs. (33)–(35) can be safely neglected provided that  $\nu'$ ,  $\epsilon'_l$ , and  $\epsilon_{\text{II}}$  satisfy the conditions listed in Eq. (32).

In RHIC HJET measurements,

$$\frac{m_0}{m_+ + m_-} \approx 0.3\%. \quad (36)$$

Therefore, the polarization determined as

$$P_{\text{BRP}} = \cos^2 \theta - \frac{m_0}{m_+ + m_-}, \quad (37)$$

yields an unbiased and precisely determined estimate of the jet target polarization,

$$P_{\text{BRP}} - P_{\text{jet}} = 2\epsilon_l - \epsilon'_l - \epsilon_{\text{II}}, \quad (38)$$

under the simplifying assumption that  $\epsilon_l = \epsilon'_l = \epsilon_{\text{II}}$  holds or, in particular, that both separating magnet systems operate with 100% efficiency.

It is important to note that the separation-magnet inefficiencies  $\epsilon_l$ ,  $\epsilon'_l$ , and  $\epsilon_{\text{II}}$  cannot be directly monitored by either the recoil spectrometer or the BRP. Consequently, establishing a reliable relation between  $P_{\text{BRP}}$  and  $P_{\text{jet}}$  requires detailed simulations of hydrogen atom trajectories through the complete HJET magnetic system.

### 3.4. Discussion

In evaluating  $P_{\text{BRP}}$ , we did not consider measurements with both RF transitions switched off. In this case, the BRP signal may be approximated as

$$\tilde{m}_0 = (1 - \nu') + (1 + \nu') = 2. \quad (39)$$

Since

$$m_+ + m_- = m_0 + \tilde{m}_0, \quad (40)$$

the measurement of  $\tilde{m}_0$  cannot improve the accuracy of the BRP determination of  $P_{\text{jet}}$ . In recent RHIC HJET measurements, it was found that

$$\langle \epsilon \rangle + \epsilon'_l + \epsilon_{\text{II}} = \frac{m_+ + m_- - \tilde{m}_0}{m_+ + m_-} \approx -0.43\%, \quad (41)$$

whereas

$$\langle \epsilon \rangle + \epsilon'_l + \epsilon_{\text{II}} = \frac{m_0}{m_+ + m_-} \approx 0.29\%. \quad (42)$$

The discrepancy, which is significant compared to the value of  $m_0$ , may be explained by a small nonlinearity at the level of approximately 0.7% in the response of the ion gauge to the measured atomic hydrogen flux intensity.

The original RHIC HJET design [24] assumed the use of a second RF unit (located in chamber 8) for BRP calibration.

However, it was later found that, owing to the small observed value of  $\langle \epsilon \rangle$ , this additional RF unit is not required [25] to determine the jet target polarization with an accuracy of approximately 0.1%. Assuming  $\epsilon_I = \epsilon'_I = \epsilon_{II} = 0$  and using Eq. (42), together with another recent BRP measurement,

$$\nu' + \frac{\epsilon_{13} - \epsilon_{24}}{2} = \frac{m_- - m_+}{m_+ + m_-} \approx 0.7\%, \quad (43)$$

one readily finds that the values of  $\nu'$ ,  $\epsilon_{13}$ , and  $\epsilon_{24}$  satisfy the conditions (32). Consequently, the equality  $P_{\text{BRP}} = P_{\text{jet}}$  is achieved with sufficient accuracy.

This conclusion remains valid in the more general case in which

$$2\epsilon_I \approx \epsilon'_I + \epsilon_{II}. \quad (44)$$

However, since the BRP measurements are not sensitive to the value of  $\epsilon_I$ , one must rely on simulations of atomic hydrogen tracking in the HJET system. In this context, BRP measurements performed with both SFT and WFT transitions turned on in both RF units,

$$m'_0 = 2\epsilon_{II}, \quad (45)$$

may be particularly useful for tuning and validating the simulation software.

In Ref. [22], it was suggested to use atomic beam blockers to completely reject states  $|3\rangle$  and  $|4\rangle$ . For the estimates presented here, such rejection corresponds to  $\epsilon'_I \rightarrow 0$  and  $\epsilon_{II} \rightarrow 0$ . As a result, the BRP would measure the unbiased RF-transition inefficiency  $\langle \epsilon \rangle$ . However, it was not fully appreciated that the effective jet polarization in the scattering chamber remains affected by  $\epsilon_I$ , leading to a biased BRP evaluation of the jet target polarization when  $\epsilon_I \neq 0$ .

Therefore, the installation of atomic beam blockers does not necessarily improve the accuracy of the determination of  $P_{\text{jet}}$ . Once again, this emphasizes the importance of accurate simulations of atomic hydrogen tracking. From this perspective, a comparison of BRP measurements performed with and without blockers may be of critical importance.

## 4. Beam-induced depolarization

In the analysis of beam-induced depolarization, we use the EIC flattop beam parameters listed in Table 1.

### 4.1. Bunch-induced magnetic field

Assuming a Gaussian longitudinal bunch density, the temporal structure of the EIC polarized proton beam current,  $I_b(t)$ , can be approximated as

$$I_b(t) = I_{\text{pk}} \sum_{k=-\infty}^{\infty} \exp\left[-\frac{(t - k\tau_b)^2}{2\sigma_t^2}\right], \quad (46)$$

where  $\tau_b$  is the bunch spacing and  $\sigma_t$  is the rms bunch length in time.

Equation (46) can also be used to describe the time dependence of the beam-induced magnetic field,  $B_{\text{ind}}(r, t)$ , provided

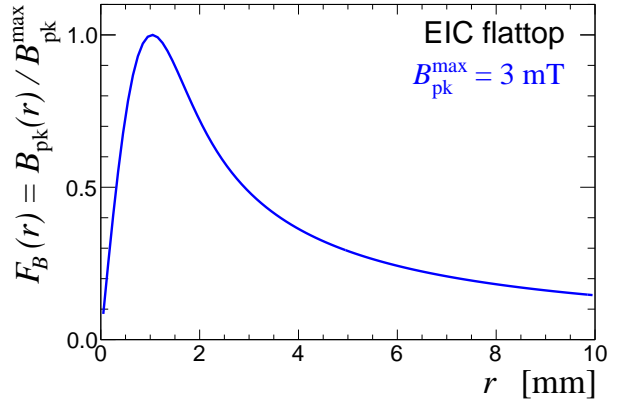


Figure 3: Unity-normalized radial profile of the beam-induced magnetic field at the EIC flattop.

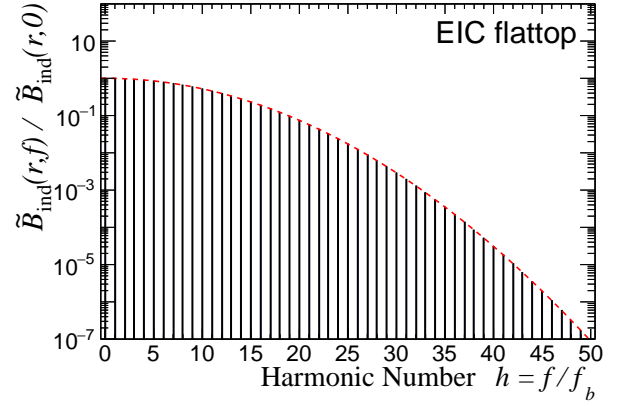


Figure 4: Fourier spectrum of the proton beam longitudinal profile planned for the EIC. The red dashed line represents the Gaussian envelope defined in Eq. (49).

that the peak current

$$I_{\text{pk}} = \frac{eN_p}{\sqrt{2\pi}\sigma_t} \approx 22 \text{ A} \quad (47)$$

is replaced by the corresponding peak magnetic field  $B_{\text{pk}}(r)$  at radial distance  $r$  from the beam axis.

Assuming a Gaussian longitudinal bunch density, the temporal structure of the EIC polarized proton beam current  $I_b(t)$  can be approximated as

$$B_{\text{pk}}(r) = \frac{\mu_0 I_{\text{pk}}}{2\pi r} \left(1 - e^{-r^2/2\sigma_r^2}\right) = B_{\text{pk}}^{\text{max}} F_B(r), \quad (48)$$

where  $\mu_0 = 4\pi \times 10^{-7} \text{ T m/A}$  is the vacuum magnetic permeability,  $B_{\text{pk}}^{\text{max}} \approx 3 \text{ mT}$  for the EIC flattop beam, and  $F_B(r)$  is a unity-normalized radial profile shown in Fig. 3.

The Fourier transform  $B_{\text{ind}}(r, t) \rightarrow \tilde{B}_{\text{ind}}(r, f)$  yields a discrete, equidistant set of  $\delta$ -function harmonics with spacing  $f_b = 1/\tau_b$ , modulated by a Gaussian envelope, as illustrated in Fig. 4. The

rms width of this envelope is

$$\sigma_f = \frac{1}{2\pi\sigma_t} \approx 796 \text{ MHz.} \quad (49)$$

Consequently, the beam-induced magnetic field at radius  $r$  can be expressed as a sum of harmonic components,

$$B_{\text{ind}}(r, t) = B_{\text{osc}}^{\max} F_B(r) \left[ 1 + \sum_{h=1}^{\infty} 2 e^{-(\omega_h \sigma_t)^2/2} \cos(\omega_h t) \right], \quad (50)$$

where  $\omega_h = 2\pi h f_b$ , and

$$B_{\text{osc}}^{\max} = B_{\text{pk}}^{\max} \frac{2\pi\sigma_t}{\tau_b} \approx 0.136 \text{ mT.} \quad (51)$$

#### 4.2. Matrix elements for bunch-induced transitions

For a hydrogen atom subjected to a weak oscillating magnetic field  $\mathbf{B}_\omega \cos(\omega t)$ , the perturbation enters the Hamiltonian as

$$H_1(t) = -\mu_e \left[ B_{\parallel} \begin{pmatrix} 1 & 0 \\ 0 & -1 \end{pmatrix}_e + B_{\perp} \begin{pmatrix} 0 & 1 \\ 1 & 0 \end{pmatrix}_e \right] \cos(\omega t), \quad (52)$$

where  $B_{\parallel}$  and  $B_{\perp}$  are the components of the oscillating magnetic field parallel and perpendicular to the holding field, respectively. The Pauli matrices act only on the electron spin.

The parallel component  $B_{\parallel}$  induces  $\sigma$  transitions ( $\Delta F = \pm 1$ ,  $\Delta m_F = 0$ ). Following Ref. [26], the corresponding matrix elements can be written as

$$\mathcal{M}_{ij}^{\sigma} = \mu_{ij}^{\sigma} B_{\parallel}, \quad \mu_{ij}^{\sigma} = 2\mu_e \begin{pmatrix} 1 & 0 & 0 & 0 \\ 0 & \cos 2\theta & 0 & -\sin 2\theta \\ 0 & 0 & -1 & 0 \\ 0 & -\sin 2\theta & 0 & -\cos 2\theta \end{pmatrix}. \quad (53)$$

The appearance of diagonal matrix elements in Eq. (53) can be understood by considering the zeroth harmonic of the beam-induced field, corresponding to the average longitudinal field  $\langle B_{\text{ind}}^{\parallel} \rangle$ . For example, retaining only the term  $\mathcal{M}_{11} = \mu_{11}^{\sigma} \langle B_{\text{ind}}^{\parallel} \rangle$ , Eq. (9) reduces to

$$i\hbar d \ln a_1 = \int \mathcal{M}_{11}(t) dt. \quad (54)$$

This results in the following modification of the phase of the  $|1\rangle$  state:

$$\exp\left(\frac{iE_{|1\rangle}t}{\hbar}\right) \rightarrow \exp\left(\frac{iE_{|1\rangle}t}{\hbar} - \frac{i2\mu_e \langle B_{\text{ind}}^{\parallel} \rangle t}{\hbar}\right), \quad (55)$$

which reflects a shift of the  $|1\rangle$  energy level due to an effective change in the holding field caused by the zeroth-harmonic component of the beam-induced field.

Therefore, the diagonal matrix elements in Eq. (53) can be neglected, provided that the time-dependent variation of the effective holding field,

$$B_{\text{hold}}^{\text{eff}}(r, t) = B_{\text{hold}} + B_{\text{ind}}(r, t) \frac{x}{r}, \quad (56)$$

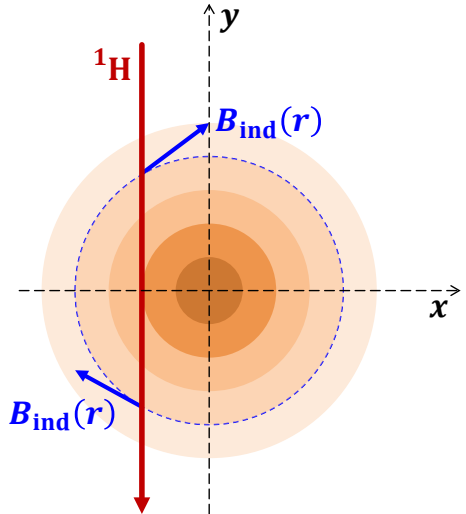


Figure 5: Tracking of a hydrogen atom through the  $z$ -directed proton beam.

(where the coordinate  $x$  is defined in Fig. 5), is explicitly taken into account in the instantaneous eigenenergies  $E_{|i\rangle}(t)$  and in the mixing angle  $\theta(t)$ . This procedure corresponds to using time-dependent Rabi frequencies  $\omega_R(t)$  and detunings  $\Delta\omega(t) = \omega - \omega_{fi}(t)$  in Eq. (13).

Notably, the variation of the atomic energy levels is driven mainly by a coherent sum of a large number of low-frequency harmonics, whereas resonant depolarization (for the HJET holding field of 120 mT) can be induced only by a single high-frequency harmonic. As a result, these two processes can be treated independently.

For  $\pi$  transitions ( $\Delta F = 0, 1$  and  $\Delta m_F = \pm 1$ ), induced by the transverse oscillating field  $B_{\perp}$ , the matrix elements are

$$\mathcal{M}_{ij}^{\pi} = \mu_{ij}^{\pi} B_{\perp}, \quad \mu_{ij}^{\pi} = 2\mu_e \begin{pmatrix} 0 & \sin \theta & 0 & \cos \theta \\ \sin \theta & 0 & \cos \theta & 0 \\ 0 & \cos \theta & 0 & -\sin \theta \\ \cos \theta & 0 & -\sin \theta & 0 \end{pmatrix}. \quad (57)$$

#### 4.3. Tracking of hydrogen atoms through the beam region

For an accurate evaluation of beam-induced transition probabilities, the trajectory of a hydrogen atom through the beam-induced magnetic field must be taken into account. If, at  $t = 0$ , the atomic coordinates are  $x_{\text{at}}(0)$  and  $y_{\text{at}}(0)$  (see Fig. 5), and the atom moves vertically with velocity  $v_{\text{at}}$ , its coordinates and radial distance from the beam axis at time  $t$  are given by

$$x_{\text{at}}(t) = x_{\text{at}}(0), \quad (58)$$

$$y_{\text{at}}(t) = y_{\text{at}}(0) - v_{\text{at}}t, \quad (59)$$

$$r_{\text{at}}(t) = \sqrt{x_{\text{at}}^2(t) + y_{\text{at}}^2(t)}. \quad (60)$$

Considering a transition  $|i\rangle \rightarrow |f\rangle$  driven by the  $h$ th beam harmonic of the beam-induced magnetic field ( $\omega_h = 2\pi h f_b$ ), the

instantaneous driving frequencies along the atomic trajectory are

$$\omega_R(t) = \frac{B_{\text{osc}}^{\max} F_B(r_{\text{at}}(t))}{\hbar r_{\text{at}}(t)} e^{-2(\pi\hbar\sigma_f/\tau_b)^2} \begin{cases} \mu_{fi}^\sigma x_{\text{at}}(t), & \sigma \text{ transitions,} \\ \mu_{fi}^\pi y_{\text{at}}(t), & \pi \text{ transitions,} \end{cases} \quad (61)$$

$$\Delta\omega(t) = \omega_h - 2\pi f_{fi} \left( B_{\text{hold}}^{\text{eff}}(r_{\text{at}}(t), t) \right), \quad (62)$$

where  $f_{fi}(B_{\text{hold}}^{\text{eff}})$  is the transition frequency determined by the instantaneous effective holding field.

Substituting  $\omega_R(t)$  and  $\Delta\omega(t)$  into Eqs. (13), one can calculate the evolution of the probability amplitudes  $\alpha_i(t)$  and  $\alpha_f(t)$  along the atomic trajectory through the beam.

In the HJET geometry, the region of significant beam-induced magnetic field is limited by the scattering chamber height,  $L_{\text{int}} = 60$  mm. Assuming that the  $z$ -directed proton beam axis is located at  $x_{\text{beam}} = y_{\text{beam}} = 0$ , the initial vertical coordinate of the hydrogen atom is taken as

$$y_{\text{at}}(0) = +\frac{L_{\text{int}}}{2}, \quad (63)$$

and the tracking is terminated when the atom reaches

$$y_{\text{at}}(t) = -\frac{L_{\text{int}}}{2}. \quad (64)$$

The horizontal coordinate  $x_{\text{at}}(0)$  of the atoms is distributed according to the jet density profile [10],

$$\frac{dN}{dx} \propto \exp\left(-\frac{x^2}{2\sigma_{\text{jet}}^2}\right), \quad (65)$$

with  $\sigma_{\text{jet}} \approx 2.6$  mm.

According to the evaluation of the atomic velocity distribution in Ref. [22], the vertical velocity  $v_{\text{at}}$  follows

$$\frac{dN}{dv_{\text{at}}} \propto v_{\text{at}}^2 \exp\left[-\frac{(v_{\text{at}} - v_{\text{drift}})^2}{2\sigma_v^2}\right], \quad (66)$$

where  $v_{\text{drift}} \approx 1800$  m/s and  $\sigma_v \approx 400$  m/s.

A typical interaction time can thus be estimated as

$$t_{\text{int}} = \frac{L_{\text{int}}}{v_{\text{drift}}} \approx 33 \mu\text{s}. \quad (67)$$

## 5. Estimated depolarization of the HJET target at EIC

Resonant depolarization may occur when a harmonic  $h$  of the beam-induced magnetic field coincides with a hyperfine transition frequency,

$$f_{ij}(B_{\text{hold}}) = hf_b, \quad (68)$$

which imposes a constraint on the choice of the holding field  $B_{\text{hold}}$ .

Using Eqs. (5), one readily finds that, for the EIC parameters, a change of the holding field by only  $\Delta B_{\text{hold}} = 3.2$  mT shifts the transition frequency  $f_{13}$  by one harmonic unit,  $f_b$ . A similar

Table 2: Transition frequencies (in units of  $f_b$ ) for the EIC flattop beam as functions of the holding field  $B_{\text{hold}}$ . The last column shows the relative suppression factor due to the Gaussian spectral envelope, evaluated at  $B_{\text{hold}} = 129$  mT.

	$f_{ij}/f_b$			$\exp(-f_{ij}^2/2\sigma_f^2)$
	126 mT	129 mT	132 mT	
$f_{12}^\pi$	6.316	6.348	6.380	$7.70 \times 10^{-1}$
$f_{34}^\pi$	9.348	9.315	9.284	$5.69 \times 10^{-1}$
$f_{23}^\pi$	32.624	33.518	34.414	$6.79 \times 10^{-4}$
$f_{22}^\pi$	38.940	39.867	40.794	$3.30 \times 10^{-5}$
$f_{13}^\sigma$	41.972	42.834	43.698	$6.71 \times 10^{-6}$
$f_{24}^\sigma$	48.288	49.182	50.078	$1.51 \times 10^{-7}$
$f_{14}^\pi$				

sensitivity to the holding field is observed for the  $f_{14}$ ,  $f_{23}$ , and  $f_{24}$  transitions.

Since the beam-induced magnetic field modifies the effective holding field by up to  $\pm 3$  mT (depending on the transverse coordinates  $x$  and  $y$ ), some hydrogen atoms will inevitably satisfy resonant transition conditions while traversing the scattering chamber, as illustrated in Table 2. The holding field value  $B_{\text{hold}} = 129$  mT considered for the EIC differs from the 120 mT used at RHIC. As demonstrated below,  $B_{\text{hold}} = 129$  mT corresponds to a local minimum of the overall beam-induced depolarization.

Nevertheless, even at zero detuning, the depolarization transition probability given by Eq. (12) may remain small.

This behavior is due to the suppression of the Rabi frequency  $\omega_R$  [see Eq. (61)] by the exponential factor  $\exp(-f_{ij}^2/2\sigma_f^2)$ , as well as to the possible smallness of the effective resonance time  $t_{\text{res}} \ll t_{\text{int}}$ . The latter arises from the explicit dependence of the beam-induced magnetic field  $B_{\text{ind}}(r, t)$  on both the atomic coordinates and time. Consequently, a reliable evaluation of the  $|i\rangle \rightarrow |f\rangle$  transition probability (assuming  $\alpha_i(0) = 1$  and  $\alpha_f(0) = 0$ ) requires an explicit time-dependent calculation of  $\alpha_f(t)$  along the hydrogen atom trajectory.

In such a study, three transition probabilities are of particular interest:

$w_{ij}^{\text{brp}}$  — the transition probability  $|\alpha_f(t)|^2$  evaluated at the exit of the interaction region,  $y = -L_{\text{int}}/2$ . This quantity is relevant for estimating the depolarization correction to the polarization determined by the Breit–Rabi polarimeter (BRP).

$w_{ij}^{\text{jet}}$  — the transition probability  $|\alpha_f(t)|^2$  convoluted with the transverse proton beam density profile. It provides an estimate of the effective depolarization of the jet target relevant for the proton beam polarization measurement.

$w_{ij}^{\text{max}}$  — the maximum value of  $|\alpha_f(t)|^2$  attained along the hydrogen atom trajectory through the region of the beam-induced magnetic field. The quantity  $(w_{ij}^{\text{max}})^{1/2}$  may be used as a practical criterion for determining whether the transition  $|i\rangle \rightarrow |j\rangle$  can be safely neglected in the system of equations (9).

Although  $w_{ij}^{\text{brp}}$ ,  $w_{ij}^{\text{jet}}$ , and  $w_{ij}^{\text{max}}$  are referred to below as depolarization probabilities, the actual change in the population (and

Table 3: Dependence of the average  $f_{23}^\pi$  transition probabilities  $w_{23}^{\text{brp}}$ ,  $w_{23}^{\text{jet}}$ , and  $w_{23}^{\text{max}}$  on the holding field  $B_{\text{hold}}$ , the initial transverse coordinate  $x(0)$  of the hydrogen atom, and its velocity  $v_{\text{at}}$ . The value  $B_{\text{hold}} = 130.6137$  mT corresponds to the exact resonant condition  $f_{23} = 34f_b$  for the  $|2\rangle \rightarrow |3\rangle$  transition in the absence of beam-induced fields. A reference to an equation in the table indicates that the corresponding parameter is distributed according to that equation.

	$B_{\text{hold}}$ [mT]	$x(0)$	$v_{\text{at}}$	$w_{23}^{\text{brp}}$	$w_{23}^{\text{jet}}$	$w_{23}^{\text{max}}$
1	130.6137	0	$v_{\text{drift}}$	$1.4 \times 10^{-9}$	$3.6 \times 10^{-4}$	$4.0 \times 10^{-4}$
2	130.6137	0	Eq. (66)	$1.6 \times 10^{-9}$	$3.4 \times 10^{-4}$	$3.8 \times 10^{-4}$
3	130.6137	Eq. (65)	$v_{\text{drift}}$	$1.2 \times 10^{-4}$	$1.0 \times 10^{-4}$	$1.4 \times 10^{-4}$
4	129	Eq. (65)	$v_{\text{drift}}$	$5.8 \times 10^{-12}$	$2.9 \times 10^{-10}$	$5.9 \times 10^{-10}$

polarization) of the atomic state  $|i\rangle$  is given by

$$P_{|i\rangle} \rightarrow P_{|i\rangle}(1 - w_{ij}) + P_{|j\rangle}w_{ij} = P_{|i\rangle} + w_{ij}(P_{|j\rangle} - P_{|i\rangle}). \quad (69)$$

Notably,  $w_{24} = 0.5$  corresponds to complete depolarization of a proton for an atom initially in the state  $|2\rangle$ , whereas  $w_{24} = 1$  corresponds to a full proton spin flip. In contrast, for the transition  $2 \rightarrow 3$ , the case  $w_{23} = 1$  changes the proton polarization from  $-\cos 2\theta$  to  $-1$ .

### 5.1. Potentially resonant transitions

According to Table 2, three transitions,  $f_{23}^\pi$ ,  $f_{24}^\sigma$ , and  $f_{14}^\pi$ , can be regarded as *potentially resonant*, meaning that an exact resonance condition may be satisfied while a hydrogen atom traverses the proton beam. The  $f_{13}$  transition is not considered here, since it corresponds to  $\Delta m_F = 2$  and is forbidden within the dipole approximation adopted in this work.

Assuming an exactly resonant holding field  $B_{\text{hold}}^{\text{res}}$ , such that  $f_{ij}(B_{\text{hold}}^{\text{res}}) = hf_b$  (prior to beam-induced corrections), and using the maximum possible Rabi frequency,

$$\omega_R^{\text{max}} = \frac{\mu_{ij} B_{\text{osc}}^{\text{max}}}{\hbar} \exp[-2(\pi\hbar\sigma_t/\tau_b)^2], \quad (70)$$

one obtains an upper bound on the depolarization transition probability,

$$w_{ij}^{\text{upper}} = \left( \frac{\omega_R^{\text{max}} t_{\text{int}}}{2} \right)^2. \quad (71)$$

For the  $f_{23}^\pi$  transition,  $B_{\text{hold}}^{\text{res}} = 130.6137$  mT, yielding

$$w_{23}^{\text{upper}} \simeq 5 \times 10^{-2}, \quad (72)$$

which, by itself, does not exclude a substantial resonant transition probability.

A more accurate analysis, including the dependence on the initial atomic coordinate  $x(0)$ , atomic velocity  $v_{\text{at}}$ , and the nominal holding field  $B_{\text{hold}}$ , as well as on the variations of  $\omega_R$  and  $\Delta\omega$  along the atomic trajectory, is summarized in Table 3.

For the resonant holding field and trajectories with  $x(0) = 0$  (lines 1 and 2 of Table 3), the values of  $w_{23}^{\text{brp}}$  are extremely small and are consistent with the numerical accuracy of the calculation. Along such trajectories, the beam-induced magnetic field is always horizontal and does not modify the  $f_{23}^\pi$  transition frequency, maintaining  $\Delta\omega = 0$ . Moreover, due to the antisymmetry of the induced field with respect to the  $y = 0$  axis, the net

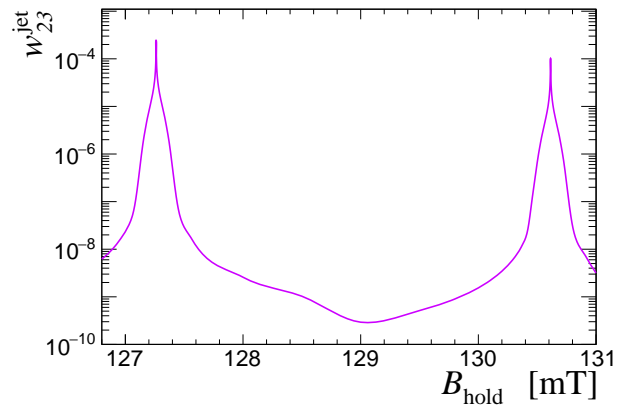


Figure 6: The recoil-spectrometer-observed  $|2\rangle \rightarrow |3\rangle$  transition probability as a function of the holding magnetic field.

effect of the evolution governed by Eqs. (13) vanishes identically for atomic motion from  $y = L_{\text{int}}/2$  to  $y = -L_{\text{int}}/2$ .

Lines 1 and 2 also demonstrate that incorporating the atomic velocity distribution does not significantly alter the estimated depolarization relative to calculations performed with a fixed velocity  $v_{\text{at}} = v_{\text{drift}}$ . Consequently, all subsequent simulations were performed using a fixed atomic velocity in order to reduce computational time.

Including the jet density profile results in transition probabilities of order  $\mathcal{O}(10^{-4})$  for  $w_{23}^{\text{brp}}$ ,  $w_{23}^{\text{jet}}$ , and  $w_{23}^{\text{max}}$ , even for the resonant holding field. A modest deviation of  $B_{\text{hold}}$  from the resonant value suppresses the transition probability to a completely negligible level, as illustrated in Fig. 6.

For the remaining *potentially resonant* transitions,  $f_{24}^\sigma$  and  $f_{14}^\pi$ , negligible beam-induced depolarization follows directly from the upper-limit estimate (71):

$$w_{24}^{\text{upper}} = 8 \times 10^{-7}, \quad (B_{\text{hold}} = 129.5785 \text{ mT}, h = 43), \quad (73)$$

$$w_{14}^{\text{upper}} = 5 \times 10^{-9}, \quad (B_{\text{hold}} = 128.3898 \text{ mT}, h = 49). \quad (74)$$

Thus, none of the *potentially resonant* transitions can produce a measurable change in the jet target polarization at the EIC, and all such transitions can be safely excluded from the system of equations (9).

## 5.2. Non-resonant transitions

With only two remaining (*non-resonant*) transitions,  $f_{12}^\pi$  and  $f_{34}^\pi$ , the four-level system (9) naturally decomposes into two independent two-level subsystems. In this case, evaluation of  $w_{ij}^{\max}$  is no longer required.

Applying Eq.(15) to these *non-resonant* transitions, one finds that in both cases the generalized Rabi frequency can be treated as approximately constant,  $\Omega/2 \approx 95$  MHz, while the instantaneous Rabi frequency satisfies  $|\omega_R(t)| \lesssim 3$  MHz and varies along the atomic trajectory. Let  $\tilde{\omega}_R(\Delta t) = \omega(t-t_0)$ , where  $t_0$  denotes the time at which the atomic trajectory crosses the  $y = 0$  plane. Then  $\tilde{\omega}_R(\Delta t)$  is an odd function of  $\Delta t$ , and for trajectories with  $x(t) = 0$ ,

$$|\tilde{\omega}_R(\Delta t)| \propto F_B(v_{\text{at}}|\Delta t|). \quad (75)$$

Using Fig. 3, one can readily estimate the characteristic Fourier frequencies  $\Omega_R$  associated with the temporal variation of  $\omega_R(t)$ :

$$\Omega_R \lesssim \frac{\pi}{2} \frac{v_{\text{at}}}{\text{mm}} \approx 3 \text{ MHz} \ll \frac{\Omega}{2}. \quad (76)$$

Thus,  $\omega_R(t)$  may be regarded as a slowly varying function of time, which justifies the use of Eq. (15) as a reasonable approximation for the pre-evaluation of the *non-resonant* transition probability  $w_{\text{non-res}}^{\text{brp}}$ . Within this approach,

$$w_{\text{non-res}}^{\text{brp}} = \frac{\omega_R^2 (L_{\text{int}}/v_{\text{at}})}{2\Omega^2} \approx 0. \quad (77)$$

A more accurate estimate, based on numerical solutions of Eqs. (13) with time-dependent  $\omega_R(t)$  and  $\delta\omega(t)$ , yields

$$w_{\text{non-res}}^{\text{brp}} \sim 0.02 w_{\text{non-res}}^{\text{jet}}. \quad (78)$$

Thus, acknowledging that the Breit–Rabi polarimeter does not possess sufficient sensitivity to detect depolarization effects arising from the *non-resonant* transitions  $f_{12}^\pi$  and  $f_{34}^\pi$ , we focus below on the corresponding jet-target depolarization relevant for recoil spectrometer measurements.

For each transition, two neighboring harmonics  $h$  and  $h+1$  satisfying

$$h < \frac{f_{ij}}{f_b} < h+1 \quad (79)$$

were taken into account. The results are presented in Fig. 7.

The total jet-target depolarization, as observed in recoil spectrometer measurements,

$$\Delta_{\text{dep}}|P_{\pm}| \approx -w_{\text{non-res}}^{\text{jet}} = -w_{12(6)}^{\text{jet}} - w_{12(7)}^{\text{jet}} - w_{34(9)}^{\text{jet}} - w_{34(10)}^{\text{jet}}, \quad (80)$$

was found to be approximately  $-0.008\%$  for the HJET holding field  $B_{\text{hold}} = 129$  mT and  $-0.011\%$  for  $B_{\text{hold}} = 120$  mT. Both values are well below the assumed precision  $O(0.1\%)$  of the jet-target polarization determination using the Breit–Rabi polarimeter.

For completeness, we also evaluate the potential depolarization in the vicinity of the resonant holding-field values corresponding to the  $f_{12}^\pi$  and  $f_{34}^\pi$  transitions. The calculated transi-

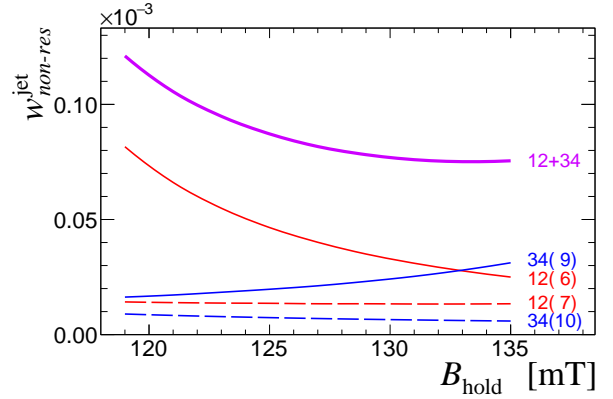


Figure 7: Calculated transition probabilities for the *non-resonant*  $f_{12}^\pi$  and  $f_{34}^\pi$  transitions as functions of the holding magnetic field. The transitions are labelled by the initial/final state  $if$  and harmonic ( $h$ ) numbers. “12+34” means the sum of all four *non-resonant* probabilities.

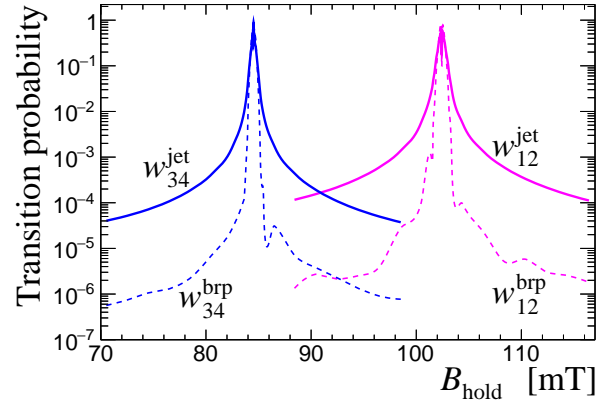


Figure 8: Calculated transition probabilities  $w^{\text{jet}}$  and  $w^{\text{brp}}$  for the  $f_{12}^\pi$  and  $f_{34}^\pi$  transitions in the vicinity of the corresponding resonant values of the holding magnetic field.

tion probabilities  $w^{\text{brp}}$  and  $w^{\text{jet}}$  for both transitions are shown in Fig. 8.

For  $B_{\text{hold}} \approx 120.45$  mT, the transition probability reaches its maximal possible value,  $w_{12}^{\text{jet}} = 1$ , corresponding to a complete spin flip of an atom initially in the state  $|1\rangle$ , i.e., full conversion  $|1\rangle \rightarrow |2\rangle$ . Consequently, this would imply complete depolarization of the jet target if it were formed by atoms in states  $|1\rangle$  and  $|4\rangle$  corresponding to polarization  $P_+$ .

In contrast to the *non-resonant* holding-field range, the BRP-related probability  $w_{12}^{\text{brp}}$  may also become large (up to unity) in the resonant case. However, since the states  $|1\rangle$  and  $|2\rangle$  have the same electron spin projection  $+1/2$ , such depolarization cannot be detected by the Breit–Rabi polarimeter unless the second RF unit—which was not employed during RHIC HJET operation—is used.

A similar conclusion applies to the  $f_{34}^\pi$  transition at  $B_{\text{hold}} \approx 84.52$  mT. In this case, however, the resulting depolarization cannot be detected by the BRP even if the second RF unit were to be used in the measurement.

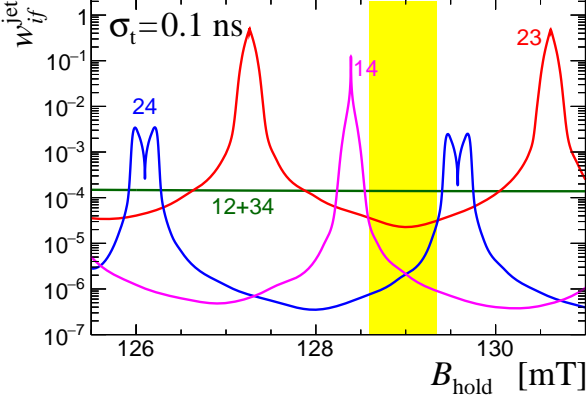


Figure 9: Transition probabilities as functions of the holding magnetic field for  $\sigma_t = 0.1$  ns. The shaded region indicates the holding-field range  $128.6 < B_{\text{hold}} < 129.35$  mT, within which the overall depolarization is negligibly small.

## 6. Stability of the evaluated depolarization against variations of the proton beam parameters

### 6.1. Reduced temporal bunch length

As shown above, the strong suppression of resonant beam-induced depolarization is primarily due to the smallness of the exponential factor entering the Rabi frequency,

$$\omega_R \propto \exp(-2\pi^2 f_{ij}^2 \sigma_t^2). \quad (81)$$

Therefore, for a fixed holding field  $B_{\text{hold}}$  (and hence a fixed transition frequency  $f_{ij}$ ), a reduction of the rms temporal bunch length  $\sigma_t$  may substantially increase the jet-target depolarization.

To estimate this effect, the dependence of the transition probabilities on  $B_{\text{hold}}$  was evaluated for all considered transitions assuming  $\sigma_t = 0.1$  ns, which is a factor of two smaller than the nominal EIC value. The results are shown in Fig. 9.

For a resonant transition, the probability (12) can be written as

$$w_{\text{res}}^{\text{jet}} = \sin^2\left(\frac{\omega_R t_{\text{int}}}{2}\right) = \frac{1}{2} - \frac{1}{2} \cos(\omega_R t_{\text{int}}). \quad (82)$$

In the regime  $\omega_R t_{\text{int}} \gg 1$ , and after averaging over a large ensemble of hydrogen atoms, the oscillatory term is effectively canceled due to variations in  $v_{\text{at}}$ ,  $x(0)$ , and the relative phase between atomic trajectories and the bunch structure.

Consequently, the limiting value  $w_{\text{res}}^{\text{jet}} = 0.5$  observed for the  $f_{23}^{\sigma}$  transition in Fig. 9 corresponds to complete saturation of the transition, i.e. to equal populations of the initial state  $|2\rangle$  and the final state  $|3\rangle$ .

For the  $\sigma$  transition  $f_{24}^{\sigma}$ , both  $\omega_R$  and  $\Delta\omega$  are primarily determined by the vertical component of the beam-induced magnetic field  $B_{\text{ind}}^{(y)}(r, t)$ . Since  $B_{\text{ind}}^{(y)}$  changes sign for  $x(0) < 0$  and  $x(0) > 0$ , the resonance condition is satisfied at two slightly different values of  $B_{\text{hold}}$ , resulting in a characteristic double-peak structure clearly visible in Fig. 9.

Although the depolarization probabilities for  $\sigma_t = 0.1$  ns are significantly larger than those obtained for the nominal

Table 4: Dependence of the *non-resonant* depolarization probability on the beam current and transverse beam size for  $B_{\text{hold}} = 129$  mT.

$I_{\text{avg}}$ [A]	$\sigma_r$ [mm]	$B_{\text{pk}}^{\text{max}}$ [mT]	$w_{\text{non-res}}^{\text{jet}}$
1	0.656	3	$7.82 \times 10^{-5}$
5	0.656	15	$1.95 \times 10^{-3}$
1	0.131	15	$1.94 \times 10^{-3}$

$\sigma_t = 0.2$  ns, depolarization-free operation of the HJET remains possible provided that the magnetic field in the scattering chamber is maintained within

$$B_{\text{hold}} = 129 \pm 0.35 \text{ mT}, \quad (83)$$

prior to beam-induced corrections.

A further reduction of  $\sigma_t$  would require a corresponding increase of the holding field (and hence of the transition frequencies  $f_{ij}$ ) in order to suppress resonant depolarization. Such a scenario is undesirable, since increasing  $B_{\text{hold}}$  would lead to a noticeable increase of systematic uncertainties in proton beam polarization measurements performed with the HJET recoil spectrometer.

### 6.2. Increased beam current

The dependence of the *non-resonant* depolarization probability on the beam parameters can be approximately expressed as

$$w_{\text{non-res}}^{\text{jet}} \propto B_{\text{ind}}^{\text{max}} 2 \propto \left(\frac{I_{\text{avg}}}{\sigma_r}\right)^2, \quad (84)$$

where  $I_{\text{avg}}$  is the average beam current and  $\sigma_r$  is the rms beam radius.

Thus, increasing  $I_{\text{avg}}$  (or decreasing  $\sigma_r$ ) by a factor of five is expected to increase the depolarization probability by approximately a factor of 25. To verify this scaling, dedicated calculations were performed, and the results are summarized in Table 4.

The results confirm that the scaling (84) provides a reliable estimate. Even for a fivefold increase of the average beam current (assuming unchanged  $\sigma_t$  and  $\sigma_r$ ), the resulting depolarization of  $\sim 2 \times 10^{-3}$  remains fairly comfortable within the EIC polarization accuracy requirement (1).

### 6.3. Elliptical beam profile

The planned 255 GeV EIC proton beam has an elliptical transverse profile,

$$I(x, y) \propto \frac{1}{2\pi\sigma_x\sigma_y} \exp\left(-\frac{x^2}{2\sigma_x^2} - \frac{y^2}{2\sigma_y^2}\right), \quad (85)$$

with  $\sigma_x = 1.610$  mm and  $\sigma_y = 0.268$  mm.

For simplicity, the calculations presented above assumed a round beam with rms radius  $\sigma_r = (\sigma_x\sigma_y)^{1/2}$ , which could potentially distort the estimate of the beam-induced depolarization.

According to the Ampère-Maxwell law,

$$\oint \mathbf{B} \cdot d\mathbf{s} = \mu_0 I, \quad (86)$$

the circulation of the magnetic field is determined by the total enclosed current. For a strongly elongated beam ( $\sigma_y \ll \sigma_x$ ), the induced magnetic field near the jet is systematically smaller than that produced by a round beam with the same rms radius  $\sigma_r$ . Therefore, the actual depolarization is expected to be lower than that evaluated assuming a round beam.

To quantify this effect, the beam-induced magnetic field  $\mathbf{B}_{\text{pk}}(x, y)$  for an elliptical current distribution was calculated numerically and used in the hydrogen-atom tracking. For the *non-resonant* transitions and  $B_{\text{hold}} = 129$  mT, the resulting depolarization was found to be

$$w_{\text{non-res}}^{\text{jet}} = 4.76 \times 10^{-5}, \quad (87)$$

which is a factor of 1.6 lower than the corresponding value in Table 4 obtained within the round-beam approximation.

## 7. Summary

In this work, the possibility of beam-induced depolarization of the HJET target in the EIC environment has been evaluated.

As a prerequisite for this study, the methods used to determine the jet target polarization with the Breit-Rabi polarimeter and to apply this polarization in the recoil spectrometer were compared. It was noted that, for the determination of the proton beam polarization with the recoil spectrometer, only the average magnitude of the jet spin-up and spin-down polarizations,  $|P_{\pm}|$ , is required. Consequently, Eq. (37) can be used for a precise evaluation of the jet target polarization  $P_{\text{jet}}$ . Since the ratio (36) is very small, even relative systematic uncertainties of order 50% in its determination can be regarded as negligible.

To evaluate beam-induced depolarization of the jet target, atomic hydrogen was treated as a four-level hyperfine system in an external (holding) magnetic field, perturbed by a time-dependent magnetic field generated by the bunched proton beam. Two main effects were considered: transitions between hyperfine levels induced by a high-frequency beam harmonic resonant with a given transition frequency, and an effective modification of the holding field (and, consequently, of the atomic energy levels) caused by the coherent contribution of low-frequency harmonics.

First, it was demonstrated that resonant conditions that may occur during the tracking of hydrogen atoms through the scattering chamber do not lead to significant transitions, because the corresponding high-frequency harmonics do not carry sufficient power for the nominal EIC flattop beam parameters.

Under these conditions, the four-level hydrogen system naturally separates into two independent two-level subsystems,  $|1\rangle-|2\rangle$  and  $|3\rangle-|4\rangle$ . Although the beam-induced field harmonics driving these transitions are substantially stronger, the corresponding resonance conditions can be readily avoided by an appropriate choice of the holding field  $B_{\text{hold}}$ .

The evolution of these subsystems during atomic traversal through the proton beam was evaluated by numerically solving Eqs. (13), with time-dependent Rabi frequencies  $\omega_R(t)$  and detunings  $\Delta\omega(t)$ .

As a result, for the nominal EIC proton beam at flattop and for the RHIC operating holding field  $B_{\text{hold}} = 120$  mT, if applied to the EIC HJET, the expected beam-induced depolarization of the jet target,

$$|\Delta_{\text{dep}} P_{\text{jet}}| \lesssim 0.01\%, \quad (88)$$

was found to be negligible.

Possible variations of the EIC flattop beam parameters that preserve this low level of depolarization were also examined.

The method employed in this work to evaluate beam-induced depolarization is analytically consistent with that used in Refs. [27, 28], where the absence of significant depolarization in polarized gas jet targets at the LHCspin [29] project was demonstrated.

A markedly different conclusion was reported in Ref. [12], where large depolarization effects were predicted for the HJET at the EIC. That result relied on the assumption that the Rabi frequency of a resonant transition is governed by an effective field amplitude of order  $B_{\text{ind}}^{\text{max}}$ , derived from a “spatial field distribution” approach. However, this analysis did not take into account that the variation frequency of the “spatial magnetic field” is fixed by the bunch frequency  $f_b$ . Consequently, for the example considered in Ref. [12], the detuning  $\Delta\omega$  exceeds the corresponding spatial-field-based Rabi frequency  $\omega_R$  by approximately a factor of 160. According to the well-justified expression in Eq. (12), the transition probability is therefore strongly suppressed in this case.

In contrast, in the present analysis the physically relevant driving field—fully consistent with the fundamental principles of induced emission and absorption in atomic systems [30]—is determined by the amplitude of the corresponding beam harmonic  $h$ ,

$$B_{\text{osc}}^{\text{max}} F_B(r) \exp[-2(\pi h \sigma_t / \tau_b)^2].$$

## Acknowledgments

The author was motivated to write this paper through numerous discussions with Frank Rathmann, Alexander Nass, and Oleg Eysen. This manuscript was authored by an employee of Brookhaven Science Associates, LLC, under Contract No. DE-SC0012704 with the U.S. Department of Energy.

## References

- [1] A. Accardi, J. L. Albacete, M. Anselmino, N. Armesto, E.-C. Aschenauer, A. Bacchetta, D. Boer, W. K. Brooks, T. Burton, N.-B. Chang, et al., Electron Ion Collider: The Next QCD Frontier, *Eur. Phys. J. A* 52 (9) (2016) 268. [arXiv:1212.1701](https://arxiv.org/abs/1212.1701), [doi:10.1140/epja/i2016-16268-9](https://doi.org/10.1140/epja/i2016-16268-9).
- [2] F. Willeke, Electron Ion Collider Conceptual Design Report 2021, Tech. Rep. BNL-221006-2021-FORE,

Brookhaven National Laboratory, Upton NY (2 2021). [doi:10.2172/1765663](https://doi.org/10.2172/1765663).

[3] R. Abdul Khalek, A. Accardi, J. Adam, D. Adamiak, W. Akers, M. Albaladejo, A. Al-bataineh, M. G. Alexeev, F. Ameli, P. Antonioli, et al., Science Requirements and Detector Concepts for the Electron-Ion Collider: EIC Yellow Report, *Nucl. Phys. A* 1026 (2022) 122447. [arXiv:2103.05419](https://arxiv.org/abs/2103.05419), [doi:10.1016/j.nuclphysa.2022.122447](https://doi.org/10.1016/j.nuclphysa.2022.122447).

[4] G. Bunce, N. Saito, J. Soffer, W. Vogelsang, Prospects for spin physics at RHIC, *Ann. Rev. Nucl. Part. Sci.* 50 (2000) 525–575. [arXiv:hep-ph/0007218](https://arxiv.org/abs/hep-ph/0007218), [doi:10.1146/annurev.nucl.50.1.525](https://doi.org/10.1146/annurev.nucl.50.1.525).

[5] E.-C. Aschenauer, A. Bazilevsky, M. Diehl, J. Drachenberg, K. O. Eyser, R. Fatemi, C. Gagliardi, Z. Kang, Y. V. Kovchegov, J. Lajoie, et al., The RHIC SPIN Program: Achievements and Future Opportunities (1 2015). [arXiv:1501.01220](https://arxiv.org/abs/1501.01220).

[6] A. N. Zelenski, G. Atoian, A. A. Bogdanov, S. B. Nurushev, F. S. Pylaev, D. Raparia, M. F. Runtso, E. Stephenson, Absolute polarimeter for the proton-beam energy of 200 MeV, *Phys. Atom. Nucl.* 76 (2013) 1490–1496. [doi:10.1134/S1063778813120156](https://doi.org/10.1134/S1063778813120156).

[7] A. Pobladuev, G. Atoian, A. Cannavo, A. Zelenski, New DAQ System for the 200 MeV Polarimeter at BNL Linac, *PoS PSTP2024* (2025) 009. [doi:10.22323/1.472.0009](https://doi.org/10.22323/1.472.0009).

[8] H. Huang, K. Kurita, Fiddling carbon strings with polarized proton beams, *AIP Conf. Proc.* 868 (2006) 3–21. [doi:10.1063/1.2401392](https://doi.org/10.1063/1.2401392).

[9] A. Zelenski, A. Bravar, D. Graham, W. Haeberli, S. Kokhanovski, Y. Makdisi, G. Mahler, A. Nass, J. Ritter, T. Wise, V. Zubets, Absolute polarized H-jet polarimeter development, for RHIC, *Nucl. Instrum. Meth. A* 536 (2005) 248–254. [doi:10.1016/j.nima.2004.08.080](https://doi.org/10.1016/j.nima.2004.08.080).

[10] A. A. Pobladuev, A. Zelenski, G. Atoian, Y. Makdisi, J. Ritter, Systematic error analysis in the absolute hydrogen gas jet polarimeter at RHIC, *Nucl. Instrum. Meth. A* 976 (2020) 164261. [arXiv:2006.08393](https://arxiv.org/abs/2006.08393), [doi:10.1016/j.nima.2020.164261](https://doi.org/10.1016/j.nima.2020.164261).

[11] A. A. Pobladuev, A. Zelenski, E. Aschenauer, G. Atoian, K. O. Eyser, H. Huang, Y. Makdisi, W. B. Schmidke, I. Alekseev, D. Svirida, N. H. Buttimore, Precision Small Scattering Angle Measurements of Elastic Proton-Proton Single and Double Spin Analyzing Powers at the RHIC Hydrogen Jet Polarimeter, *Phys. Rev. Lett.* 123 (16) (2019) 162001. [arXiv:1909.11135](https://arxiv.org/abs/1909.11135), [doi:10.1103/PhysRevLett.123.162001](https://doi.org/10.1103/PhysRevLett.123.162001).

[12] F. Rathmann, A. Nass, K. O. Eyser, V. Shmakova, E. C. Aschenauer, G. Atoian, A. Cannavo, K. Hock, H. Huang, H. Lovelace, et al., Eliminating beam-induced depolarizing effects in the hydrogen jet target for high-precision proton beam polarimetry at the Electron-Ion Collider (8 2025). [arXiv:2508.01366](https://arxiv.org/abs/2508.01366).

[13] A. Pobladuev, A. Zelenski, G. Atoian, The prospects on the absolute proton beam polarimetry at EIC, *PoS PSTP2019* (2020) 007. [doi:10.22323/1.379.0007](https://doi.org/10.22323/1.379.0007).

[14] A. Pobladuev, The Polarized Hydrogen Gas Jet Target. From RHIC to EIC., *PoS SPIN2023* (2024) 091. [doi:10.22323/1.456.0091](https://doi.org/10.22323/1.456.0091).

[15] K. Ackerstaff, A. Airapetian, N. Akopov, M. Amarian, E. C. Aschenauer, H. Avakian, R. Avakian, A. Avetissian, B. Bains, C. Baumgarten, et al., Beam induced nuclear depolarization in a gaseous polarized hydrogen target, *Phys. Rev. Lett.* 82 (1999) 1164–1168. [arXiv:hep-ex/9806006](https://arxiv.org/abs/hep-ex/9806006), [doi:10.1103/PhysRevLett.82.1164](https://doi.org/10.1103/PhysRevLett.82.1164).

[16] R. P. Feynman, R. B. Leighton, M. Sands, *The Feynman Lectures on Physics, Vol. 3*, new millennium Edition, Basic Books, 2011. URL <https://www.feynmanlectures.caltech.edu/>

[17] P. J. Mohr, D. B. Newell, B. N. Taylor, E. Tiesinga, CODATA recommended values of the fundamental physical constants: 2022\*, *Rev. Mod. Phys.* 97 (2) (2025) 025002. [arXiv:2409.03787](https://arxiv.org/abs/2409.03787), [doi:10.1103/RevModPhys.97.025002](https://doi.org/10.1103/RevModPhys.97.025002).

[18] M. Diermaier, C. B. Jepsen, B. Kolbinger, C. Malbrunot, O. Massiczek, C. Sauerzopf, M. C. Simon, J. Zmeskal, E. Widmann, In-beam measurement of the hydrogen hyperfine splitting and prospects for antihydrogen spectroscopy, *Nature Commun.* 8 (2017) 5749. [arXiv:1610.06392](https://arxiv.org/abs/1610.06392), [doi:10.1038/ncomms15749](https://doi.org/10.1038/ncomms15749).

[19] W. Haeberli, Sources of polarized ions, *Ann. Rev. Nucl. Part. Sci.* 17 (1967) 373–426. [doi:10.1146/annurev.ns.17.120167.002105](https://doi.org/10.1146/annurev.ns.17.120167.002105).

[20] L. D. Landau, E. M. Lifshitz, *Quantum Mechanics: Non-Relativistic Theory*, 3rd Edition, Vol. 3 of Course of Theoretical Physics, Pergamon Press, Oxford, 1977.

[21] I. I. Rabi, Space Quantization in a Gyrating Magnetic Field, *Phys. Rev.* 51 (8) (1937) 652. [doi:10.1103/PhysRev.51.652](https://doi.org/10.1103/PhysRev.51.652).

[22] T. Wise, M. A. Chapman, W. Haeberli, H. Kolster, P. A. Quin, An optimization study for the RHIC polarized jet target, *Nucl. Instrum. Meth. A* 556 (2006) 1–12. [doi:10.1016/j.nima.2005.09.042](https://doi.org/10.1016/j.nima.2005.09.042).

[23] C. Baumgarten, B. Braun, G. Court, G. Ciullo, P. Ferretti, A. Golendukhin, G. Graw, W. Haeberli, M. Henoch, R. Hertenberger, et al., An atomic beam polarimeter to measure the nuclear polarization in the HERMES gaseous polarized hydrogen and deuterium target, *Nucl.*

Instrum. Meth. A 482 (2002) 606–618. [doi:10.1016/S0168-9002\(01\)01738-7](https://doi.org/10.1016/S0168-9002(01)01738-7).

- [24] T. Wise, M. Chapman, W. Haeberli, D. Graham, A. Kponou, G. Mahler, Y. Makdisi, W. Meng, A. Nass, J. Ritter, A. Zelenski, S. Kokhanovski, V. Zubets, Polarized hydrogen jet target for measurement of RHIC proton beam polarization, in: 16th International Spin Physics Symposium (SPIN 2004), 2004, pp. 757–760.
- [25] A. Zelenski, private communication (2022).
- [26] J. P. M. Beijers, Adiabatic spin transitions in polarized proton sources, Nuclear Instruments and Methods in Physics Research Section A: Accelerators, Spectrometers, Detectors and Associated Equipment 536 (2005) 282–288. [doi:10.1016/j.nima.2004.08.099](https://doi.org/10.1016/j.nima.2004.08.099).
- [27] E. Steffens, [Beam-Induced Depolarization and Application to a Polarized Gas Target in the LHC beam](#), Tech. Rep. CERN-PBC-Note-2018-001, CERN, Geneva (Jul 2018).  
URL <https://cds.cern.ch/record/2632904>
- [28] P. Lenisa, E. Steffens, V. Carassiti, G. Ciullo, P. Di Nezza, L. Pappalardo, A. A. Vasilyev, LHCspin: a polarized internal target for the LHC, PoS PSTP2019 (2020) 025. [doi:10.22323/1.379.0025](https://doi.org/10.22323/1.379.0025).
- [29] A. Accardi, A. Bacchetta, L. Barion, G. Bedeschi, V. Benesova, S. Bertelli, V. Bertone, C. Bissolotti, M. Boglione, G. Bozzi, et al., LHCspin: a Polarized Gas Target for LHC (4 2025). [arXiv:2504.16034](https://arxiv.org/abs/2504.16034).
- [30] V. B. Berestetskii, E. M. Lifshitz, L. P. Pitaevskii, Quantum Electrodynamics, Volume 4 (Course of Theoretical Physics), 2nd Edition, Course of Theoretical Physics, Pergamon Press / Butterworth–Heinemann, Oxford, United Kingdom, 1982, translated from the Russian by J. B. Sykes and J. S. Bell.